Surface-Fluorinated Proton-Exchange Membrane with High Electrochemical Durability for Direct Methanol Fuel Cells

Chang Hyun Lee,[†,‡] So Young Lee,[†] Young Moo Lee,[*,†] Sang Yun Lee,[§] Ji Won Rhim,[||] Ozma Lane,[‡] and James E. McGrath[‡]

School of Chemical Engineering, College of Engineering, Hanyang University, Seoul 133-791, Korea, Macromolecules and Interface Institute, Virginia Polytechnic Institute and State University, Blacksburg, Virginia 24061, Department of Civil and Environmental Engineering, Korea Advanced Institute of Science and Technology, Daejeon 305-701, Korea, and Department of Chemical Engineering, Hannam University, Daejeon 306-791, Korea

ABSTRACT Random disulfonated poly(arylene ether sulfone)—silica nanocomposite (FSPAES-SiO_2) membranes were physicochemically tuned via surface fluorination. Surface fluorination for 30 min converted about 20% of the C—H bonds on the membrane surface into C—F bonds showing hydrophobicity and electronegativity at the same time. The membranes with hydrophobic surface properties showed high dimensional stability and low methanol permeability when hydrated for direct methanol fuel cell applications. In particular, the surface enrichment of fluorine atoms led to anisotropic swelling behavior, associated with a stable electrode interface formation. Interestingly, in spite of the use of a random copolymer as a polymer matrix, the low surface free energy of the C—F bonds induced a well-defined continuous ionic channel structure, similar to those of multiblock copolymers. In addition to the morphological transition, fluorine atoms with high electron-withdrawing capability promoted the dissociation of sulfonic acid (—SO_3H) groups. Consequently, FSPAES-SiO_2 membranes exhibited improved proton conductivity. Thus, FSPAES-SiO_2 membranes exhibited significantly improved single-cell performances (about 200%) at a constant voltage of 0.4 V in comparison with those of Nafion 117 and nonfluorinated membranes. Surprisingly, their good electrochemical performances were maintained with very low nonrecovery loss over the time period of 1400 h and interfacial resistances 380% times lower than those of conventional membrane—electrode assemblies comprising the control hydrocarbon membrane and a Nafion binder for the electrodes.

KEYWORDS: proton-exchange membrane • surface fluorination • interfacial resistance • membrane—electrode assembly • electrochemical durability • direct methanol fuel cell

INTRODUCTION

Direct methanol fuel cells (DMFCs) are highlighted as promising power sources for portable electronic devices owing to their high energy density (5—10 times larger than current lithium-ion batteries) and simple system (1). A key element that determines the electrochemical performances of DMFCs is the membrane—electrode assembly (MEA) composed of a proton-exchange membrane (PEM) and the electrodes. Up to now, perfluorinated sulfonic acid (PFSA) membranes (e.g., Nafion) have been widely used as PEM materials because of their excellent membrane durability and proton conductivity (2). However, PFSA membranes exhibit a high methanol crossover problem, and as methanol permeates through the membranes, one notes lowered catalyst activity and fuel cell performances. This negative behavior is clearly observed especially at high operating temperatures and/or when using high methanol concentrations (3). This characteristic has prevented DMFC systems that utilize PFSA membranes from maintaining high electrochemical performances for a long period of time.

In contrast, some sulfonated hydrocarbon polymeric membranes show excellent methanol barrier properties and proton conduction properties similar to or higher than those of PFSAs (4—7). The hydrocarbon membranes display DMFC performances superior to those of PFSA for short periods of fuel cell operation. However, their current—voltage performances may rapidly decrease within several days. To overcome this limitation on lifetime, it is necessary to better understand the hydrocarbon-based MEA (HC-MEA) and its components. Generally, ionomer materials are added to the electrode's formula as a catalyst binder to physically support catalyst-containing carbon clusters and to facilitate the migration of protons from the electrode to the membrane and vice versa (8). For this purpose, Nafion ionomer (EW = 1100) has been conventionally used, irrespective of which electrolyte membrane is employed. Unlike MEAs based on PFSA membranes, the use of Nafion binders in an HC-MEA gives rise to serious interfacial issues including high resistance and poor adhesion derived from low compatibility with hydrocarbon membranes (9). Consequently, it leads to

* Corresponding author. Tel.: +82-2-2220-0525. Fax: +82-2-2291-5982. E-mail: ymlee@hanyang.ac.kr.
Received for review February 2, 2009 and accepted April 13, 2009
† Hanyang University.
‡ Virginia Polytechnic Institute and State University.
§ Korea Advanced Institute of Science and Technology.
|| Hannam University.
DOI: 10.1021/am900067q

the delamination of catalyst layers from the hydrocarbon membrane and, thus, rapid electrochemical losses during DMFC operation cycles when both the membrane and catalyst binder are repeatedly swollen and deswollen.

There have been extensive studies to solve the interfacial problems between MEA components, in particular between a membrane and electrodes, from the viewpoint of hydrocarbon membranes. For instance, identical materials with hydrocarbon membranes were used as catalyst binders instead of Nafion ionomers (10). In spite of much improved compatibility with the membranes, the hydrocarbon binder had relatively low fuel permeability, which limits mass transport, resulting in a reduced electrochemical performance. The other approach is the chemical modification of membrane materials via the incorporation of partially or fully fluorinated monomers for a minimum interfacial resistance with Nafion-based electrodes (11−13). However, the cost of fluorinated monomer is relatively high, which may make the merits of fluorinated copolymers less attractive (14).

In this study, a new platform that enables the fabrication of fuel cell membranes having high compatibility with electrodes and excellent electrochemical durability via simple, rapid conversion of surface properties of hydrocarbon membranes into those similar to fluorinated membranes is described. This approach, termed "surface fluorination", can expand the processing window for less expensive and possibly more durable HC-PEMs in conjunction with MEA fabrication. Surface fluorination has been important for automobiles (15), packing (16), food storage and preservation (17), gas separation (18), and coating applications (19) because it enables surface-treated hydrocarbon polymers to exhibit most of the desirable properties of fluoropolymers (i.e., chemical durability and good barrier property), while maintaining their useful bulk properties such as easy processability and high mechanical properties. Previously, an investigation to improve the thermal and chemical stability of PEM materials after concentrated F_2 gas treatment for a relatively long period of time (~24 h) was conducted using a partially fluorinated monomer (20). However, there have been no reports to promote PEM properties such as proton conductivity and methanol permeability via surface fluorination of nonfluorinated hydrocarbon membranes for a relatively short time (<30 min) and to apply the process to hydrocarbon membranes to enable high current−voltage performance without decreases in their interfacial properties even for a long period. Accordingly, the main goal of the present study was to systematically show the effect of surface fluorination on basic PEM properties and to demonstrate its contribution to the electrochemical fuel cell performance.

EXPERIMENTAL SECTION

Chemicals. 4,4′-Dichlorodiphenylsulfone (DCDPS) and 4,4′-dihydroxybiphenyl (BP) used for synthesizing poly(arylene ether sulfone) BPSH40 random copolymer were purchased from Tokyo Kasei Co. (Tokyo, Japan) and used after recrystallization with ethanol and vacuum drying at 120 °C for 24 h. DCDPS was sulfonated to 3,3′-disulfonated DCDPS (SDCDPS; yield = 91.4%) through monomer sulfonation by using SO_3 (28%, Aldrich, Madison, WI). *N*-Methylpyrrolidinone (NMP) and dimethylacetamide (DMAc; Aldrich Chemical Co., Madison, WI) were used as a solvent for polymer synthesis and a casting solvent, respectively. Potassium carbonate was purchased from Aldrich Chemical Co. and used as received. Pluronic L64 (PEO_{13}−PPO_{30}−PEO_{13}; BASF, Ludwigshafen, Germany) was used as a dispersant to distribute nanoparticles homogeneously. Nanosized fumed SiO_2 Aerosil 380 was purchased from Degussa Chemical Co. (Dusseldorf, Germany) and dried at 80 °C and 3−5 mmHg for 2 days prior to use.

Membrane Fabrication and Surface Fluorination. A disulfonated poly(arylene ether sulfone) BPSH random copolymer−silica nanocomposite (SPAES-SiO_2) as a base membrane material was prepared via consecutive two-step reactions: (1) polycondensation for the synthesis of BPSH40 as a polymer matrix with a chemical structure of Figure S1 in the Supporting Information using SDCDPS (4 mmol), DCDPS (6 mmol), and BP (10 mmol) in NMP (21) and (2) physical mixing with a DMAc solution mixture composed of Aerosil 380 and Pluronics L64 as a nonporous inorganic nanoparticle (hydrophilic silica, average size = 7 nm) and dispersant, respectively (22). The successful synthesis of BPSH40 was confirmed via ^{1}H NMR (Figure S1 in the Supporting Information). Here, the silica content was 1 wt % based on the polymer weight. A SPAES-SiO_2 membrane with an average thickness of 30 μm was obtained after casting of a 15 wt % solution on the glass plate, drying at 60 °C for 8 h, and thermal treatment at 80 °C for 24 h, 100 °C for 6 h, and 120 °C for 8 h in a vacuum oven. Then, the membrane was acidified in a boiling 0.5 M H_2SO_4 solution for 2 h and thoroughly washed in boiling water for 2 h (method II). The SPAES-SiO_2 membranes were treated with a dilute F_2 gas (500 ppm F_2/N_2 at atmospheric pressure) at 25 °C for 5, 10, 30, and 60 min in a reaction chamber. The degree of fluorination was constant on both sides of the membranes. To terminate the surface fluorination reaction, the unreacted F_2 gas was removed by alternately applying a vacuum and N_2 gas to the chamber. In this study, the surface-treated nanocomposite membranes are denoted as FSPAES-SiO_2 -surface fluorination time on a scale of minutes. For instance, FSPAES-SiO_2-5 means a SPAES-SiO_2 membrane surface-treated for 5 min.

Characterization. X-ray photoelectron spectroscopy (XPS) spectra were obtained in survey mode and high-resolution mode using monochromatic Al Kα radiation as the X-ray source under normal pressure below 7×10^{-9} Torr. The survey measurement was accomplished with 10 sweeping cycles in the electron binding energy ranges of 0−800 eV. The high-resolution XPS spectra were obtained from an average of 100 scans for C 1s and O 1s peaks. The detected spot size of the membrane samples was 250×1000 μm^2. An electron flood gun (operation voltage = 3 eV) was used to minimize the charge from membranes.

Instantaneous contact-angle measurements were carried out with an Easy Drop Standard (KRU″SS, Hamburg, Germany) instrument using the sessile-drop method. The drop image was stored by a video camera, and the contact angle was obtained by an image analysis system from the shape of the drop. Deionized water was used as a probe. For each sample, five drops were analyzed on each membrane substrate. The average volume of the drops was about 2 μL. The final contact angle was obtained by an average of the right and left angles of each drop.

Atomic force microscopy (AFM) images in the tapping mode were obtained by using a Digital Instruments MultiMode scanning probe microscope with a NanoScope IVa controller. For imaging of the samples, a silicon probe (Veeco, end radius <10 nm) was used at a force constant of 5 N m^{-1}. The experimental conditions include a set-point ratio of 0.82. Prior to the mea-

Table 1. Basic Physical and Fuel Cell Membrane Properties of SPAES-SiO_2 and FSPAES-SiO_2 Membranes

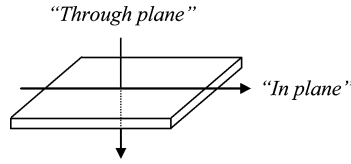

	XPS quantitative analysis					
sample	F [%]	F/C × 100 [%]	IEC[a] [mequiv g^{-1}]	water uptake[b] [%]	in-plane swelling[b] [%]	through-plane swelling[b] [%]
SPAES-SiO_2			1.60	25.4	20.2	18.8
FSPAES-SiO_2-5	3.7	5	1.59	23.2	18.3	19.9
FSPAES-SiO_2-10	9.2	12	1.58	21.9	16.1	21.2
FSPAES-SiO_2-30	13.5	19	1.58	20.4	13.7	23.6
FSPAES-SiO_2-60	14.9	21	1.58	20.3	12.6	24.3

[a] The titration method was based on ASTM 2187. [b] Measured at 30 °C after soaking in deionized water for 1 day.

surement, each sample was equilibrated at 30 °C and 40% relative humidity for 12 h.

Mechanical properties of SPAES-SiO_2 and FSPAES-SiO_2-30 membranes (50 mm and 4 mm of length and minimum width in a dogbone shape, respectively) were evaluated using an Instron 5500R universal testing machine (Instron Ltd., Canton, MA, USA) at 25 °C and 44−54% relative humidity (RH). For this, 200 lb of load cell was used and the crosshead displacement speed was 5 mm min^{-1}. Prior to the measurement, each sample was dried at 110 °C under vacuum for at least 12 h and, then, equilibrated at 25 °C and 44% RH. At least five specimens were tested for each membrane.

The water uptake (%) of all membranes was measured based on their weight difference after soaking of the membrane coupons with a constant size (5 × 5 cm^2) in deionized water at 30 °C for 24 h, as shown in eq 1.

$$W = \frac{W_w - W_d}{W_d} \quad (1)$$

where W_d and W_w are the masses of the dry and water-swollen samples, respectively.

The "in-plane" and "through-plane" swelling (%) of each membrane were evaluated by comparing the changes in its diameter and thickness before and after equilibrium water uptake (eqs 2 and 3). Prior to measurement, each membrane coupon was dried in a vacuum oven at 120 °C for 24 h and immersed in deionized water at 30 °C for 24 h

$$d = \frac{d_w - d_d}{d_d} \quad (2)$$

$$l = \frac{l_w - l_d}{l_d} \quad (3)$$

where d_d and d_w are the diameters of the dry and water-swollen samples, respectively, and l_d and l_w are the thicknesses of the dry and water-swollen samples, respectively.

The proton conductivity (σ, S cm^{-1}) of each membrane sample (size = 1 × 4 cm^2) was obtained by measuring its ohmic resistance (R_s, Ω) in liquid water at 30 °C via a four-electrode method upon contact with the membrane surface ("in-plane" direction, Table 1) under alternating current (ac) (four-point-probe ac impedance spectroscopy using a combination of Solartron 1287 and 1260) and, thereby, converting R_s into conductivity on the basis of the equation $\sigma = l/R_sS$ (l and S are the distance between the reference electrodes and the cross-sectional area of each sample, respectively). The measurement was conducted in a thermocontrolled chamber electrically shielded from the influence of electromagnetic noises.

The concentration gradient of methanol diffused from one chamber to another chamber through a vertical membrane was measured with a gas chromatograph (Shimadzu GC-14B, Tokyo, Japan) equipped with a thermal conductivity detector (two-chamber diffusion cell method). Here, each chamber was filled with 10 M MeOH and deionized water at 30 °C. The methanol permeability (P, cm^3 cm cm^{-2} s^{-1}) of each membrane sample was obtained from eq 4

$$P = \frac{V_B L}{C_A A} \frac{C_B(t)}{t} f \quad (4)$$

where V_B is the initial volume of deionized water in one chamber, L is the membrane thickness, A is the membrane area, C_A is the initial methanol concentration in another chamber, $C_B(t)$ is the methanol concentration as a function of time (t), and f is the conversion factor by gas chromatography calibration.

The electronic resistance (Ω) of each MEA [e.g., high-frequency resistance (HFR)] was obtained by measuring the whole resistance of the test cell (i.e., including current collectors, flow fields, gas diffusion layers, electrodes, and a membrane) based on two-point-probe ac impedance spectroscopy with potentiometers as mentioned above. Here, a current up to 30 A was applied to the test cell in a direction perpendicular ("through plane", Table 1) to the membrane surface. Each measurement was carried out repeatedly at least five times to ensure good reproducibility.

RESULTS AND DISCUSSION

Surface Fluorination. Generally, highly reactive F_2 gas reacts easily with most organic and inorganic materials even at room temperature via complicated radical-chain reaction mechanisms (23). This makes it difficult to estimate the exact location of fluorination on the surface-treated SPAES-SiO_2 membranes. Among feasible reaction routes, hydrogen abstraction by fluorine is thermodynamically favorable because the C−H bond strength (410 kJ mol^{-1}) is much lower than any other bond strength between elements (i.e., aromatic C−C bond strength = 610 kJ mol^{-1}) in the membranes. Thus, it can be expected that surface fluorination on SPAES-SiO_2 membranes will induce random C−F bond formation.

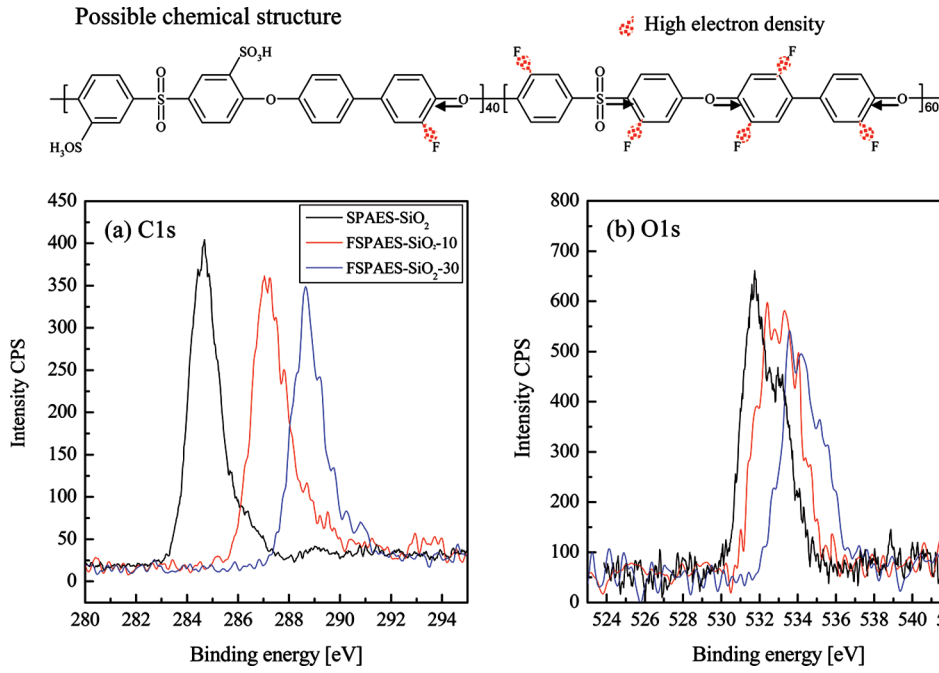

FIGURE 1. XPS narrow spectra for (a) C 1s and (b) O 1s in high-resolution mode.

The fluorinated layer has been reported to form with an average thickness of 0.1−10 μm after surface fluorination using dilute gas mixtures of F_2 and inert gases (24). Considering that the X-ray penetration depth in XPS is more than 1 μm (25), it may be very effective to verify surface fluorination on the SPAES-SiO_2 membrane qualitatively and quantitatively based on XPS spectra. The survey spectra of the SPAES-SiO_2 membrane are observed to be made up of peaks assigned as O 1s (~530 eV), C 1s (~283 eV), S 2s (228 eV), S 2p (170 eV), Si 2p (~93 eV), and Si 2s (~143 eV) (Figure S2 in the Supporting Information). FSPAES-SiO_2 membranes have an additional characteristic peak assigned as F 1s at around 686 eV. Moreover, the fluorine content in FSPAES-SiO_2 membranes increased with exposure time to F_2 gas, as shown in Table 1. About 20% of C−H bonds located on the surface of the SPAES-SiO_2 membrane are converted into C−F bonds after F_2 gas exposure of about 30 min. This conversion may alter the electron density of the elements adjacent to C−F bonds mainly in the phenyl ring because of the high electronegativity (4.0) of fluorine. Figure 1 shows changes in the binding energies of carbon and oxygen in FSPAES-SiO_2 membranes as a function of the surface fluorination times. The C 1s peak at 285 eV was shifted upfield to 289 eV. As a result of C−F bond formation, the emission of photoelectrons from carbon directly linked with fluorine becomes more difficult. Accordingly, additional energy (ca. 4 eV) is needed to excite their electrons. A similar trend is also observed in the oxygen binding energy. The gap in its binding energy is relatively small (ca. 2 eV) as compared with that of carbon. This means that electrons around oxygen atoms bridged with phenyl rings are less influenced by the electron-withdrawing fluorine atoms. Meanwhile, no chemical shifts of silicon and sulfur atoms were observed in XPS spectra (Figure S2 in the Supporting Information). This means that SiO_2 nanoparticles in the composite are inert

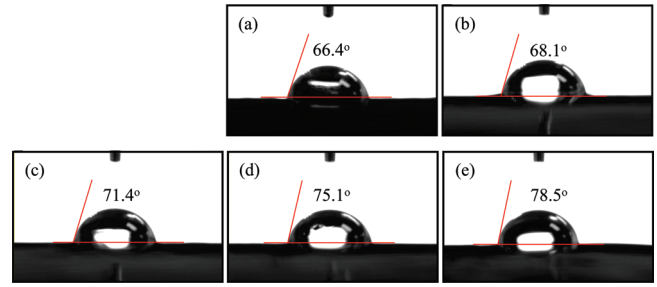

FIGURE 2. Water contact angle of (a) SPAES-SiO_2, (b) FSPAES-SiO_2-5, (c) FSPAES-SiO_2-10, (d) FSPAES-SiO_2-30, and (e) FSPAES-SiO_2-60.

under the fluorination conditions. It also indicates that fluorination occurs only on the surface of the random copolymer. The sulfonic acid (−SO_3H) groups in the polymer main chains appear to be also free from F_2 gas attack. Consequently, the ion-exchange capacity (IEC) values of FSPAES-SiO_2 membranes are similar to that of the control SPAES-SiO_2 membrane (Table 1).

Instantaneous water contact-angle measurement was used to confirm the change in the hydrophobicity of the membrane surface. Figure 2 shows that the contact angle increases after surface fluorination. The higher contact angle associated with the fluorination time is attributed to an increasing amount of hydrophobic C−F bonds at the surface of the FSPAES-SiO_2 membranes.

The AFM phase images in Figure 3 indicate that surface fluorination can induce a fairly well-defined microphase separation on the membrane surface. In the SPAES-SiO_2 membrane, hydrophilic clusterlike structures (dark region) with an average diameter of 5−15 nm are distributed with some local connection in the hydrophobic copolymer matrix (light region), similar to those of random statistical copolymers (21). The phase images in FSPAES-SiO_2 membranes undergo considerable morphological changes. The hydro-

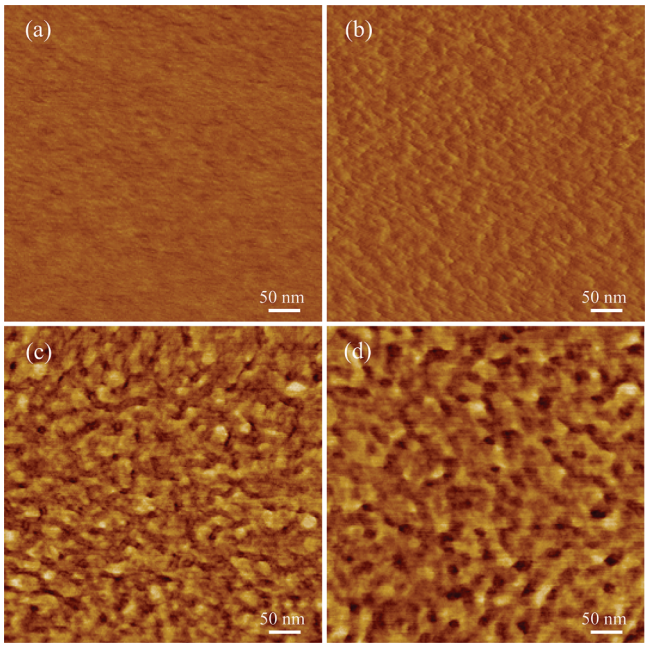

FIGURE 3. AFM phase images of (a) SPAES-SiO_2, (b) FSPAES-SiO_2-10, (c) FSPAES-SiO_2-30, and (d) FSPAES-SiO_2-60 membranes in tapping mode. Here, scan boxes are 500 × 500 nm^2. The phase scale is 0−20° for parts a and b and 0−30° for parts c and d. The relative humidity for the measurement is about 35% RH.

philic ionic domains became connected to produce clear, large continuous ionic channels as the time of fluorination increased up to 30 min. This suggests that the low surface free energy of C−F bonds acts as a dynamic driving force for self-assembly on the partially fluorinated membrane surface. However, surface fluorination longer than 30 min did not cause any further changes in the connectivity or channel size of hydrophilic domains, which implies that surface treatment for 30 min at these thicknesses may be optimal to altering the transport properties of the membranes. Moreover, it is hypothesized that most surface fluorination may be achieved mainly on hydrophobic domains in the random copolymer rather than on its hydrophilic domains, considering that the surface treatment was conducted with SPAES-SiO_2 membranes in the dry state where the membrane surface is more hydrophobic. This is why the continuous morphology similar to those of hydrophilic−hydrophobic multiblock copolymers is observed after surface fluorination (26).

Meanwhile, surface fluorination did not change the mechanical properties, which are bulk characteristics of membrane materials. For example, FSPAES-SiO_2-30 membranes maintained their tough and ductile properties, showing a tensile strength (69 MPa) and elongation (40%) similar to those of the SPAES-SiO_2 membrane. This means that polymer chain degradation derived from F_2 gas attack (24, 27) did not occur under our surface fluorination conditions.

PEM Properties. Proton conductivity and methanol permeability are important factors influencing the electrochemical DMFC performances. Generally, proton transport through the membrane occurs in the form of complexes (H_3O^+, $H_5O_2^+$, and $CH_3OH_2^+$) with water and methanol molecules (28, 29). Therefore, excellent proton conductivity

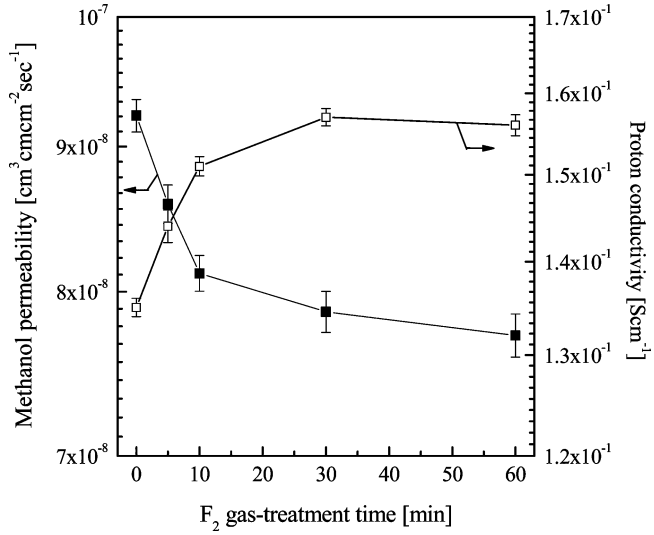

FIGURE 4. Proton conductivity and methanol permeability of SPAES-SiO_2 and FSPAES-SiO_2 membranes at 30 °C.

is accompanied by both high water uptake and low methanol barrier properties. However, surface-fluorinated membranes exhibit water uptake and transport behavior in relation to the characteristics of fluorine atoms: (1) hydrophobicity and (2) electronegativity. Table 1 shows that hydrophobic C−F groups contribute to the reduction of water uptake. The water uptake of FSPAES-SiO_2 membranes decreased to 80% of that of SPAES-SiO_2. Nevertheless, their proton conductivity in Figure 4 increased continuously until the surface fluorination time reached 30 min. One possibility is that protons can be more readily released from $-SO_3H$ groups because of improved acidity resulting from the electronegative fluorine atoms in the C−F groups. Here, it is hypothesized that the improved proton conductivity is derived from "in-plane" proton conductivity measurement with high sensitivity on the surface (30, 31). Even on the basis of "through-plane" measurement, protons in FSPAES-SiO_2 membranes can transport through a nonfluorinated inner layer and fluorinated outer double layers where protons are more effectively dissociated from the $-SO_3H$ groups. One may conclude that surface fluorination enhanced the proton conductivity, regardless of the measurement methods. Meanwhile, the hydrophobic glassy surface layers allow FSPAES-SiO_2 membranes to have high barrier properties to methanol−water mixtures. The methanol permeability decreased continuously with the fluorination extent. Highly fluorinated FSPAES-SiO_2 membranes exhibit methanol permeabilities about 20 times lower than Nafion 117 (1.4×10^{-6} cm^3cm cm^{-2} s^{-1} measured under a 10 M methanol solution at 30 °C).

Interestingly, FSPAES-SiO_2 membranes display anisotropic swelling behavior (Table 1) in that the membranes are swollen in a specific direction. It is proposed that the surface enrichment of fluorine atoms hinders the FSPAES-SiO_2 membranes from swelling in the "in-plane" direction. On the contrary, the membranes are swollen only in the "through-plane" direction owing to relatively poor fluorine enrichment. This distinctive swelling behavior may significantly influence the electrochemical durability of MEAs based on

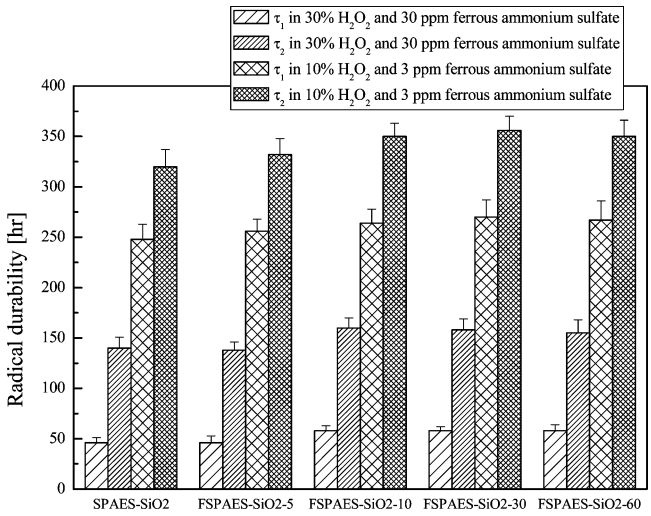

FIGURE 5. Chemical resistance to radical attack under different compositions of Fenton's solution at 25 °C. Here, τ_1 and τ_2 mean the elapsed time that the membrane samples began to dissolve and dissolved completely.

FSPAES-SiO_2 membranes. The isotropic membrane swelling maximizes the difference in the swelling ratio with electrodes containing a Nafion binder, which will likely accelerate the delamination of electrode layers. In contrast, membrane swelling in a direction perpendicular to the electrode layers may minimize the structural breakage of MEAs and, thereby, enhance fuel cell durability and performance (32).

The high chemical stability of PEM materials may also guarantee the long-term performances of fuel cells exposed under harsh conditions including hydroxyl radicals (•OH). Even PFSA membranes with excellent chemical durability have suffered from membrane degradation during fuel cell operation (33). The radical-induced membrane degradation is considered to occur more readily in hydrocarbon membranes (34, 35). For this, Fenton's solutions with two different compositions (30 ppm Fe^{2+} in 30% H_2O_2 and 3 ppm Fe^{2+} in 10% H_2O_2) were used. Here, Fenton's test may not be a reliable indicator to evaluate the chemical durability of hydrocarbon membranes. However, the test can be used to relatively compare the effect of surface fluorination on membrane stability. Figure 5 shows an example for improvement of the membrane resistance to radical attack. In spite of the low fluorine content and surface enrichment, FSPAES-SiO_2 membranes showed higher chemical durability than the control SPAES-SiO_2 membrane. Surface treatment over 5 min provided FSPAES-SiO_2 membranes with the highest level of radical resistance among hydrocarbon membranes under similar Fenton's test conditions (36). Although surface fluorination may not present a sufficient solution for radical degradation, it should enhance the radical resistance via a simple post-treatment even for a short time.

Electrochemical Performances for DMFC Application. Electrochemical single-cell data can be used to evaluate the comprehensive improvement of PEM performances when all MEAs are fabricated with the same components and composition based on identical assembly methods. Here, each MEA (active area = 5 cm^2) was fabricated through the catalyst-coated membrane method. The loading content of catalysts (Pt black for the cathode and Pt–Ru black for the anode) and the Nafion binder were 3.0 and 0.3 mg cm^{-2}, respectively. Pristine SPAES and Nafion 117 were used for comparison.

Figure 6 presents DMFC performance curves for FSPAES-SiO_2 membranes. FSPAES-SiO_2 membranes showed improved current–voltage properties because of the synergistic effect of surface fluorination on the proton-transport and methanol barrier properties. Their electrochemical performances at a constant voltage of 0.4 V are about 2 times higher than those of Nafion 117 and pristine SPAES. However, the DMFC performances did not increase linearly with the fluorination time. Practically, FSPAES-SiO_2-30 exhibited fuel cell performances superior to any other fluorinated membranes including FSPAES-SiO_2-60. This points out that effective fluorinated layers on fuel cell performances are formed within 30 min under our surface fluorination conditions.

A critical issue in current fuel cell membrane studies is the electrochemical lifetime of the membrane during fuel cell operation. Figure 7 exhibits the voltage changes at constant current density generated during a long-term DMFC operation. Note that the electrochemical durability measurement was done under harsh conditions for both the membrane and its MEA. After each cycle, the DMFC was stopped for 24 h and cooled to 25 °C without any humidification to maintain each MEA in the dry state. In the next cycle, MEA was hydrated at 90 °C, again. This repeated on–off cycle operation causes dimensional changes of MEA components, particularly polymeric materials (e.g., membrane and catalyst binder) and results in the physical breakdown of the MEA interface. Obviously, this phenomenon was observed most severely in the interfaces between the Nafion binder in the electrodes and hydrocarbon membranes. The pristine SPAES membrane interface began to delaminate within 500 h. The SPAES-SiO_2 membrane has a much improved cell voltage value because of its relatively higher proton conductivity and lower methanol permeability than those of pristine SPAES (proton conductivity = 8.4×10^{-2} S cm^{-1} in liquid water at 30 °C and methanol permeability = 6.6×10^{-7} cm^3 cm cm^{-2} s^{-1} in 10 M methanol at 30 °C). However, its decrease of the electrochemical performance per operation time (irreversible loss) is similar to that of pristine SPAES.

Compared to the control membranes, FSPAES-SiO_2 membranes display better behavior in the long-term durability curves. In addition to high initial cell voltages, their cell performances decreased only slowly. In fact, the DMFC performance of FSPAES-SiO_2-30 was sustainable even for 1400 h. Considering the very low permanent loss of FSPAES-SiO_2-30, its electrochemical lifetime may be extended further. The excellent long-term durability focusing on the membrane properties may be derived from the combination of multiple factors. Primarily, reduced methanol permeability can impede the catalyst poisoning and, hence, lead to the relatively long lifetime of electrode catalysts and corresponding MEA. Furthermore, anisotropic swelling behavior can be beneficial to produce a stable MEA interfacial

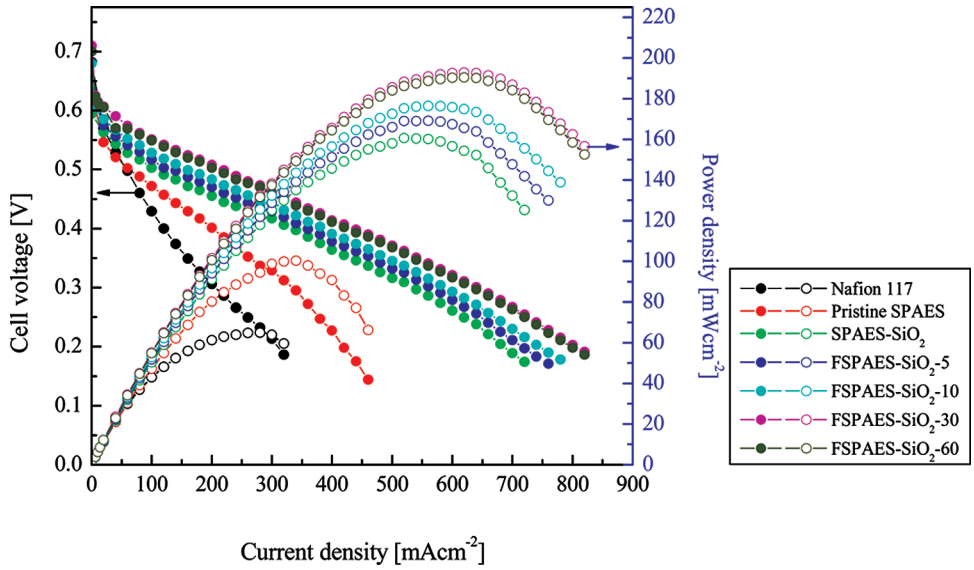

FIGURE 6. Electrochemical single-cell performances under a flow rate of 1 M methanol/O_2 = 1 sccm/200 sccm at 90 °C.

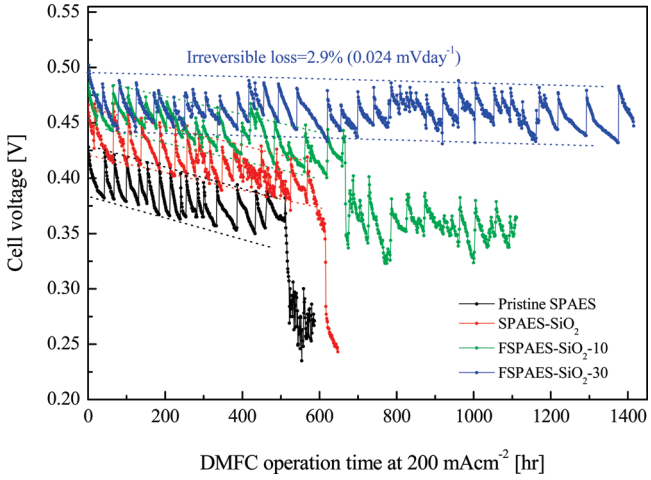

FIGURE 7. Electrochemical long-term durability of pristine SPAES, SPAES-SiO_2, and FSPAES-SiO_2 membranes under a flow rate of 1 M methanol/O_2 = 3 sccm/1000 sccm at 90 °C.

structure. Finally, C−F bond formation on the SPAES-SiO_2 membrane surface can promote compatibility with electrode layers containing the perfluorosulfonic acid Nafion binder.

Figure 8 shows changes in the HFR (Ω cm^2) of each MEA during a long-term durability test. Here, HFR as an intercept of Z' axis is the sum of all resistances in the pathway from the potentiometer to MEA. The resistance measurement was achieved by using the same test equipment and interconnection method. Here, all MEA components except membranes were identical. Thus, the differences in HFR are derived from membrane and interfacial resistance between the membrane and electrodes. Accordingly, the relative comparison of their HFR values can give valuable information for a successful MEA design. MEAs based on pristine SPAES and SPAES-SiO_2 membranes have similar resistance values owing to high interfacial resistance with the electrodes. Explicitly, HFR values of MEA based on FSPAES-SiO_2 membranes are less than half of those based on pristine SPAES and SPAES-SiO_2 membranes. Considering that proton conductivities of the nonfluorinated membranes are not half those of the fluorinated membranes, it can be concluded that this difference in HFR values is highly related to the interfacial resistance with the electrodes. The membrane surface with a high fluorine content led to much improved compatibility with the electrodes. After 1200 h of operation, their resistances were remarkably lower than the initial resistance of nonfluorinated membranes. This means that surface fluorination on hydrocarbon membranes contributes to the formation of a stable interface without significant delamination. These results provide a feasible route to improving the PEM properties and to extending the lifetime on their MEAs with excellent electrochemical performances at the same time.

CONCLUSIONS

The membrane properties of a SPAES-SiO_2 nanocomposite were improved by exposing them to highly reactive F_2 gas diluted in N_2 for a short period of over 5 min. This treatment altered, mainly, the membrane surface properties via substitution of hydrogen atoms in C−H bonds on the phenyl rings with fluorine atoms. The more hydrophobic C−F bonds on the membrane surface led to lower dimensional changes in the FSPAES-SiO_2 membranes. Also, the surface-fluorinated membranes exhibited anisotropic swelling behavior, which is highly related to the surface enrichment of C−F bonds. These peculiar swelling characteristics contributed to the improvement of methanol barrier properties and the formation of a stable interface with Nafion-based electrodes, even in the repeated swelling and deswelling cycle during DMFC operation. Concurrently, formation of the C−F bond lowered the electron density of other atoms such as carbon and oxygen adjacent to electronegative fluorine atoms and weakened the bond dissociation energy between protons and $-SO_3^-$ groups. Also, the FSPAES-SiO_2 membranes show a distinct hydrophilic−hydrophobic microphase separation with an increase in the degree of fluorination up to 30 min. Accordingly, protons could be easily released at a fast rate through continuous hydrophilic pathways in

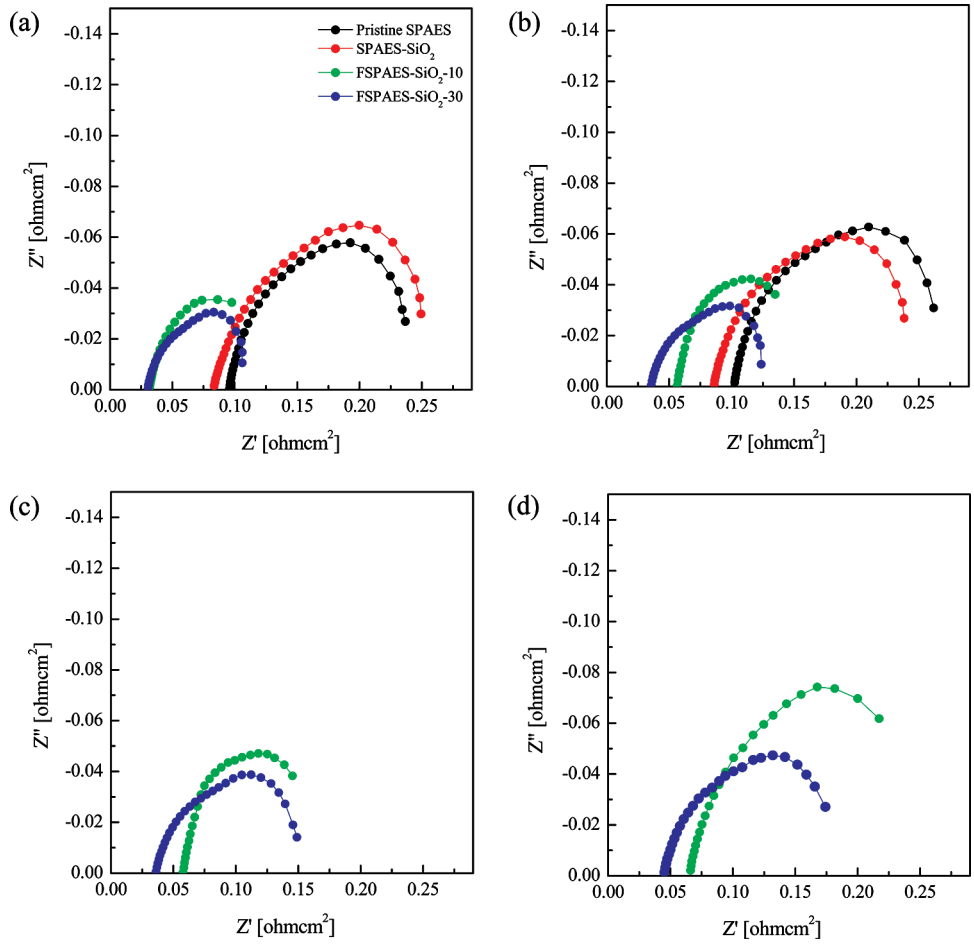

FIGURE 8. Change in HFR values of MEAs as a function of time under the long-term durability test conditions: (a) 0 h; (b) 400 h; (c) 800 h; (d) 1200 h.

FSPAES-SiO_2 membranes, similar to Nafion. In addition to enhanced proton conductivity, FSPAES-SiO_2 membranes exhibited chemical resistance similar to that of the most chemically stable hydrocarbon membranes reported. After simple post-treatment for 30 min, the single-cell performances of FSPAES-SiO_2 membranes increased up to 200% of those of nonfluorinated hydrocarbon membranes and Nafion 117 at a constant voltage of 0.4 V, owing to low methanol permeation and high proton conduction through the membranes. Surprisingly, their electrochemical performances were significantly extended up to over 1400 h, and they had extremely low irreversible loss values. The excellent electrochemical durability is attributed to high compatibility between FSPAES-SiO_2 membranes and electrode layers, anisotropic swelling behavior, and catalyst protection from poisoning by methanol.

Surface fluorination provides an effective and economical avenue to accomplishing the ultimate goals of PEM materials for practical fuel cell development as follows: (1) high single-cell performances and (2) excellent electrochemical sustainability. Surface fluorination for 30 min may be somewhat long for commercialization. Fortunately, similar results may be achieved within several minutes by controlling the degree of fluorination on the membrane surface with factors such as surface fluorination temperature and pressure and F_2 gas concentration and composition (27, 37). Moreover, this surface fluorination technique may be applied to MEA fabrication for PEM fuel cells (PEFCs) using hydrogen as the fuel. Our ongoing studies will focus on reducing the surface fluorination time while maintaining or improving membrane properties including the electrochemical performance for PEFC as well as DMFC membranes. Finally, we will attempt surface fluorination on multiblock copolymers in order to maximize the microphase or nanophase separation between hydrophilic and hydrophilic domains for more effective proton-transport pathway formation.

Acknowledgment. This work was supported by the Korea Foundation for International Cooperation of Science & Technology through a grant by the Korean Ministry of Education, Science Technology (Grant K20701010356-07B0100-10610).

Note Added after ASAP Publication. This article was released ASAP on May 1, 2009, with minor text errors. The correct version was posted on May 8, 2009.

Supporting Information Available: ^{1}H NMR spectrum of BPSH40 used as a copolymer matrix in this study (Figure S1) and XPS survey spectra of (a) SPAES, (b) SPAES-SiO_2, and (c) FSPAES-SiO_2-30 (Figure S2). This material is available free of charge via the Internet at http://pubs.acs.org.

REFERENCES AND NOTES

(1) Steele, B. C. H.; Heinzel, A. *Nature* **2001**, *414*, 345–352.
(2) Mauritz, K. A.; Moore, R. B. *Chem. Rev.* **2004**, *104*, 4535–4586.
(3) Hallinan, D. T.; Elabd, Y. A. *J. Phys. Chem. B* **2007**, *111*, 13221–13230.
(4) Asano, N.; Aoki, M.; Suzuki, S.; Miyatake, K.; Uchida, H.; Watanabe, M. *J. Am. Chem. Soc.* **2006**, *128*, 1762–1769.
(5) Tsang, E. M. W.; Zhang, Z.; Shi, Z.; Soboleva, T.; Holdcroft, S. *J. Am. Chem. Soc.* **2007**, *129*, 15106–15107.
(6) Li, Y.; Roy, A.; Badami, A. S.; Hill, M.; Yang, J.; Dunn, S.; McGrath, J. E. *J. Power Sources* **2007**, *172*, 30–38.
(7) Yamaguchi, T.; Zhou, H.; Hara, N. *Adv. Mater.* **2007**, *19*, 592–596.
(8) Borup, R.; Meyers, J.; Pivovar, B.; Kim, Y. S.; Mukundan, R.; Garland, N.; Myers, D.; Wilson, M.; Garzon, F.; Wood, D.; Zelenay, P.; More, K.; Stroh, K.; Zawodzinski, T.; Boncella, J.; McGrath, J. E.; Inaba, M.; Miyatake, K.; Hori, M.; Ota, K.; Ogumi, Z.; Miyata, S.; Nishikata, A.; Siroma, Z.; Uchimoto, Y.; Yasuda, K.; Kimijima, K.; Iwashita, N. *Chem. Rev.* **2007**, *107*, 3904–3951.
(9) Scott, K.; Taama, W. M.; Argyropoulos, P. *J. Membr. Sci.* **2000**, *171*, 119–130.
(10) Jung, H. Y.; Cho, K. Y.; Sung, K. A.; Kim, W. K.; Park, J. K. *J. Power Sources* **2006**, *163*, 56–59.
(11) Kim, Y. S.; Sumner, M. J.; Harrison, W. L.; Riffle, J. S.; McGrath, J. E.; Pivovar, B. S. *J. Electrochem. Soc.* **2004**, *151* (12), A2150—A2156.
(12) Wiles, K. B.; Diego, C. M.; Abajo, J.; McGrath, J. E. *J. Membr. Sci.* **2007**, *294*, 22–29.
(13) Sankir, M.; Kim, Y. S.; Pivovar, B. S.; McGrath, J. E. *J. Membr. Sci.* **2007**, *299*, 8–18.
(14) Nieh, M. P.; Guiver., M. D.; Kim, D. S.; Ding, J.; Norsten, T. *Macromolecules* **2008**, *41*, 6176–6182.
(15) Anand, M.; Hobbs, J. P.; Brass, I. J. *Organofluorine Chemistry: Principles and Applications*; Plenum Press: New York, 1994; p 474.
(16) Hobbs, J. P.; Anand, M.; Campion, B. A. *Barrier Polymer Structure*; ACS Symposium Series 423; American Chemical Society: Washington, DC, 1990; p 280.
(17) Kawaga, N.; Kurita, Y. JP Patent 02147640 A2, 1990.
(18) Mohr, J. M.; Paul, D. R.; Pinnau, I.; Koros, W. J. *J. Membr. Sci.* **1991**, *56*, 77–98.
(19) Dixon, D. D.; Hayes, L. J. U.S. Patent 3,988,491, 1976.
(20) Zhou, Z.; Dominey, R. N.; Rolland, J. P.; Maynor, B. W.; Pandya, A. A.; DeSimone, J. M. *J. Am. Chem. Soc.* **2006**, *128*, 12963–12972.
(21) Wang, F.; Hickner, M.; Kim, Y. S.; Zawodzinski, T. A.; McGrath, J. E. *J. Membr. Sci.* **2002**, *197*, 231–242.
(22) Lee, C. H.; Min, K. A.; Park, H. B.; Hong, Y. T.; Jung, B. O.; Lee, Y. M. *J. Membr. Sci.* **2007**, *303*, 258–266.
(23) Barsamyan, G.; Sokolov, V. B. *Fluoropolymers I: Synthesis*; Plenum Press: New York, 1999.
(24) Kharitonov, A. P.; Taege, R.; Ferrier, G.; Teplyakov, V. V.; Syrtsova, D. A.; Koops, G. H. *J. Fluorine Chem.* **2005**, *126*, 251–263.
(25) Kawai, J.; Adachi, H.; Kitajima, Y.; Maeda, K.; Hayakawa, S.; Gohshi, Y. *Anal. Sci.* **1997**, *13*, 797–801.
(26) Lee, H. S.; Roy, A.; Badami, A. S.; McGrath, J. E. *J. Polym. Sci., Part A: Polym. Chem.* **2007**, *45*, 4879–4890.
(27) Kharitonov, A. P. *J. Fluorine Chem.* **2000**, *103*, 123–127.
(28) Day, T. J. F.; Schmitt, U. W.; Voth, G. A. *J. Am. Chem. Soc.* **2000**, *122*, 12027–12028.
(29) Robeson, L. M.; Hwu, H. H.; McGrath, J. E. *J. Membr. Sci.* **2007**, *302*, 70–77.
(30) Lee, C. H.; Park, H. B.; Lee, Y. M.; Lee, R. D. *Ind. Eng. Chem. Res.* **2005**, *44*, 7617–7626.
(31) Soboleva, T.; Xie, Z.; Shi, Z.; Tsang, E.; Navessin., T.; Holdcroft, S. *J. Electroanal. Chem.* **2008**, *622*, 145–152.
(32) Lee, H. S.; Roy, A.; Lane, O.; Dunn, S.; McGrath, J. E. *Polymer* **2008**, *49*, 715–723.
(33) Lu, C.; Rice, C.; Masel, R. I.; Babu, P. K.; Waszczuk, P.; Kim, H. S.; Oldfield, E.; Wieckowski, A. *J. Phys. Chem. B* **2002**, *106*, 9581–9589.
(34) Fang, J.; Guo, X.; Harada, S.; Watari, T.; Tanaka, K.; Kita, H.; Okamoto, K.-i. *Macromolecules* **2002**, *35*, 9022–9028.
(35) Xing, P.; Robertson, G. P.; Guiver, M. D.; Mikhailenko, S. D.; Kaliaguine, S. *Macromolecules* **2004**, *37*, 7960–7967.
(36) Schuster, M.; Kreuer, K. D.; Andersen, H. T.; Maier, J. *Macromolecules* **2007**, *40*, 598–607.
(37) Sasaki, Y.; Ebara, R.; Nanbu, N.; Takehara, M.; Ue, M. *J. Fluorine Chem.* **2001**, *108*, 117–120.

AM900067Q